Determination of the cross section of the ^{39}K(n, p)^{39}Ar reaction induced by D-D neutrons with neutron activation and noble gas mass spectrometry techniques*

Xiao-Han Liu (刘笑函)[1,2] Chang-Lin Lan (兰长林)[2†] Hao-Nan Li (李昊南)[2] Bo Gao (高波)[2]
Kuo-Zhi Xu (徐阔之)[2] Jiang-Long Pan (潘江龙)[2] Xiao-Dong Pan (潘小东)[2] Wan-Feng Shi (史万峰)[2]
Bao-Chun Li (李保春)[1] Fei Su (苏菲)[3‡] Huai-Yu He (贺怀宇)[3] Jun-Jie Li (李军杰)[4]

[1]College of Physics and Electronic Engineering, Shanxi University, Taiyuan 030006, China
[2]School of Nuclear Science and Technology, Lanzhou University, Lanzhou 730000, China
[3]The Institute of Geology and Geophysics, Chinese Academy of Geological Sciences, Beijing 100029, China
[4]Beijing Research Institute of Uranium Geology, Beijing 100029, China

Abstract: The cross-sections of ^{39}K(n, p)^{39}Ar at an energy of 2–3 MeV play an important role in nuclear structure research and ^{40}Ar/^{39}Ar geochronology application. Due to the limitations of n-^{3}He coincidence technology and counting instruments, the data in literature are from before 1967, and existing data are scarce and significantly diverge. Meanwhile, there are large discrepancies between the measured and evaluation results. By taking advantage of the high sensitivity and resolution of the noble gas mass spectrometer at the Institute of Geology and Geophysics, Chinese Academy of Sciences (IGGCAS), the cross-sections of ^{39}K(n, p)^{39}Ar were measured by combining neutron activity analysis and noble gas mass spectrometry, and the uncertainties are discussed in detail. The cross-sections of ^{39}K(n, p)^{39}Ar were measured as 103.84 ± 16.33, 109.76 ± 15.88, and 150.27 ± 24.19 mb at 2.56 ± 0.08, 2.69 ± 0.08, and 2.96 ± 0.12 MeV energies, respectively. The measured data filled the data gaps and provided more accurate data support for ^{40}Ar/^{39}Ar dating. Furthermore, the theoretical excitation function of ^{39}K(n, p)^{39}Ar was calculated using TALYS-1.97 computer codes. Then, the experimentally determined cross-sections were analyzed by comparing them with the data from the EXFOR database and evaluated nuclear data in ENDF/B-VIII.0, JEFF-3.2, TENDL-2021, BROND-3.1, and JENDL-5 databases. According to the comparative results, the measured cross-sections of ^{39}K(n, p)^{39}Ar exhibit a rapid energy-dependent increase between 2–3 MeV, aligning with higher literature values and resolving previous discrepancies. Compared with the previously reported data, the precision of the determined cross-sections in this study showed considerable improvement. The comparison of measured data indicates that the combined detection method of neutron activity analysis and noble gas mass spectrometry techniques is suitable for measuring the cross-sections of nuclear reactions with long-lived product nuclei and the application of ^{40}Ar/^{39}Ar geochronology with a D-D neutron source.

Keywords: ^{39}K(n, p)^{39}Ar, cross-section, neutron activation, noble gas spectrometer

DOI: 10.1088/1674-1137/ae2f57 **CSTR:** 32044.14.ChinesePhysicsC.50044002

I. INTRODUCTION

Nuclear data play an important role in applied and nuclear physics research, and neutron cross-sections are of great significance to fusion reactors [1] and nuclear structures of nuclear reactions [2]. Moreover, the cross-section of the ^{39}K(n, p)^{39}Ar reaction is of significance to the application of ^{40}Ar/^{39}Ar dating technology. Only three studies have reported data points of the cross-sections of ^{39}K(n, p)^{39}Ar at approximately 2.5 MeV. The cross-sections of ^{39}K(n, p)^{39}Ar induced by a neutron with an energy of 2.59 MeV was measured using a D-D reactor and n-^{3}He coincidence system by Lindström [3] in 1958 for the study of the ^{39}Ar nuclear structure. The experimentally obtained cross-sections of ^{39}K(n, p)^{39}Ar were found to be 45 mb with 10% uncertainty. There was an approximately 100% deviation from the 96 ± 6 mb measured by Dixon [4] in 1961 at 2.49 MeV. Although the results exhibited a law of rapid energy-dependent increase between 2–3 MeV in Bass's [5] research, the nearly 100% devi-

Received 10 July 2025; Accepted 19 December 2025; Accepted manuscript online 20 December 2025
* Supported by the National Nuclear Energy Development Project (HNKF202327 (36)) and the National Natural Science Foundation of China (41573050).
† E-mail: lanchl@lzu.edu.cn
‡ E-mail: sufei@mail.iggcas.ac.cn

ation is evidently abnormal. Johnson replicated the experiment of Dixon in 1967 and acquired a cross-section of 95 ± 4 mb at a neutron energy of 2.46 MeV [6]. A ^{3}He long counter and KI(Tl) detector were used in the n-^{3}He coincidence system for the counts of emitted ^{3}He and ^{39}K neutron induced reactions, respectively. The ^{3}He long counter has to resolve the protons, tritons, and ^{3}He recoil particle signals of the D(d, p)T and D(d, n)^{3}He reactions from the D-D reaction. Despite considerable efforts to mitigate the influence of charged particles other than ^{3}He, the outcomes have been suboptimal. Existing methods either inadequately shield non-target charged particles or only partially attenuate non-^{3}He charged particles [7−9], thereby compromising the accuracy of the data.

The cross-sections of ^{39}K(n, p)^{39}Ar are also crucial for improving ^{40}Ar/^{39}Ar geochronology. ^{40}Ar/^{39}Ar dating is one of the most widely applied geochronological methods in Earth sciences [10]. A key step in this method involves converting ^{39}K to ^{39}Ar via neutron irradiation. The ^{40}Ar/^{39}Ar age is calculated using the following equation:

$$t = \frac{1}{\lambda}\ln\left(1 + \frac{^{40}Ar^{*}}{^{39}Ar} \times J\right), \tag{1}$$

J in Eq. (1) is

$$J = \frac{\lambda}{\lambda_{e}} \times \frac{\int \Phi(E) \times \sigma(E)\mathrm{d}E}{^{40}K/^{39}K}. \tag{2}$$

Here, E represents the energy of neutron irradiation, and $\Phi(E)$ and $\sigma(E)$ represent the neutron fluence and cross section of ^{39}K(n, p)^{39}Ar at neutron reaction energy E, respectively. ^{40}K and ^{39}K are the potassium isotope contents of the ^{40}K and ^{39}K dating samples, ^{40}Ar* is the radiogenic ^{40}Ar from ^{40}K decay, ^{39}Ar is the content of ^{39}Ar from the neutron reaction ^{39}K(n, p)^{39}Ar, λ is the total decay constant of ^{40}K, and λ_{e} is the electron capture decay constant of ^{40}K.

Typically, J is determined using samples of known age as neutron flux monitors. Renne *et al.* [11] proposed the use of D-D neutron sources in ^{40}Ar/^{39}Ar dating. Owing to the excellent mono-energetic nature of D-D neutrons, Eq. (2) can be reformulated to $J = \frac{\lambda}{\lambda_{e}} \times \frac{\Phi \times \sigma}{^{40}K/^{39}K}$, and the neutron fluence and cross-section can be directly determined by the irradiation experimental sample to get the J-value directly. The D-D neutron source mitigates issues such as interference reactions and nuclear recoil associated with the broad energy spectrum of the conventional reactor-based neutron sources [12−14]. The cross-sections of the ^{39}K(n, p) reaction in the 2–3 MeV neutron energy range are crucial for absolute ^{40}Ar/^{39}Ar dating, as this energy range corresponds to typical D-D neutron energies and exhibits a rapid increase in cross-section. However, only three data points are available around 2.5 MeV. The evaluated data of ^{39}K(n, p)^{39}Ar cross-sections in ENDF/B-VIII.0 differ from the existing experimental values by over 90%. Moreover, cross-section values from different nuclear data libraries show substantial discrepancies near 2.5 MeV. The cross-sections of ^{39}K(n, p)^{39}Ar near 2.5 MeV from ENDF/B-VIII.0, JEFF-3.3, TENDL-2021, BROND-3.1, JENDL-5, and relevant published literature are summarized in Table 1 [15−19].

In the 2–3 MeV energy range, there have been no attempts to remeasure the cross-sections of ^{39}K(n, p)^{39}Ar since 1967. Moreover, the n-^{3}He coincidence technique has problems of long counter inaccuracy caused by scattered particles at large angles and non-^{3}He signal peak overlap, which directly affect the accuracy of coincidence counts and ^{3}He total counts. As a result, the experimental cross-section data of ^{39}K(n, p)^{39}Ar around 2.5 MeV are limited, the available data differ widely, the precision of the experimental data is low, and the development of an absolute ^{40}Ar/^{39}Ar dating method is limited by poor reliability and accuracy data. Considering the divergence and scarcity of ^{39}K(n, p) cross-sections at 2–3 MeV energy and the poor accuracy, it is necessary to remeasure the cross section to fill the data gaps and provide reliable data to meet the requirements of modern experiments.

With the development of noble gas mass spectrometry technology, argon can be accurately measured. We have proposed a detection method that combines neutron activation and mass spectrometry to conduct high-precision cross-section measurements of ^{39}K(n, p)^{39}Ar instead of detecting the n-^{3}He coincidence signal. The combined method above avoids the problems of large-angle particle scattering and ^{3}He spectral overlap of the n-^{3}He coincidence system. Neutron activation analysis (NAA) is a highly mature technique used for neutron reaction energy and flux in the detection of cross-sections [20, 21]. As the most sensitive technology for the detection of argon to date, noble gas mass spectrometers have high resolution and low-concentration detection capability for Ar iso-

Table 1. Cross-sections of ^{39}K(n, p)^{39}Ar at 2–3 MeV neutron energy from available published literature and nuclear databases.

Neutron Energy/MeV	Cross-section/mb	Reference
2.59	45 with 10%	Lindström [3]
2.49	96 ± 6	Dixon [4]
2.46	95 ± 4	Johnson [6]
2.50	187.86	ENDF/B-VIII.0 [15]
2.50	163.24	JEFF-3.3 [16]
2.50	166.04	TENDL-2021 [17]
2.50	118.25	BROND-3.1 [18]
2.50	116.28	JENDL-5 [19]

topes. With the multi-collector and CFM [22, 23] (combined Faraday counting CDD (compact discrete dynode) multiplier), noble gas mass spectrometers have good precision for different mass argon isotopes (^{36}Ar, ^{37}Ar, ^{39}Ar, and ^{40}Ar) and a weak signal for ^{39}Ar, which is suitable for the detection of argon.

In the present work, a detection method for the cross-sections of ^{39}K(n, p)^{39}Ar based on the combination of neutron activation analysis (NAA) and the noble gas mass spectrometer (NGMS) technique is established. The neutron flux can be obtained using the γ-ray spectrum of the activity monitor in the neutron activation technique, and the number of ^{39}Ar reaction nuclei can be obtained by noble gas mass spectrometry. The cross-sections of ^{39}K(n, p)^{39}Ar were determined at 2.56, 2.69, and 2.96 MeV mean neutron energies using a high-sensitivity and high-resolution instrument. The reliability and precision of measured cross-sections was considered by comparison with previous literature data, evaluated data of databases, and TALYS-1.97 theoretical calculation data.

II. EXPERIMENT

A. Theoretical formula

The cross-sections of ^{39}K(n, p)^{39}Ar were determined by measuring the full-energy peak of monitor (^{58}Ni) characteristic γ-ray and the ^{39}Ar content of the activated sample. The potassium samples sandwiched with nickel monitors were irradiated by neutrons emitted from D(d, n)^{3}He. The gamma spectrum of activated nickel samples was obtained by an off-line γ-ray spectrometric technique with high resolution and a low background HPGe detector for the determination of neutron fluence. Then, the ^{39}Ar content of irradiated samples was measured by noble gas mass spectrometer. According to the definition of cross-sections, the measurement equation is as follows:

$$\sigma = \frac{N_{\mathrm{Ar}}}{N_{\mathrm{K}}\Phi}, \tag{3}$$

where $\Phi = \varphi T$ is total neutron fluence; φ is the neutron flux; T is the total irradiation time; N_{Ar} is the number of moles of ^{39}Ar from the ^{39}K(n, p) reaction; N_{K} is the number of moles of ^{39}K from the target sample; and N_{Ar} represents the number of nuclear reactions.

B. Neutron source

The irradiation was performed using the CPNG-600 neutron generator at China Institute of Atomic Energy (CIAE). The time of irradiation was approximately 94.5 h. The neutrons were produced by D(d, n)^{3}He reaction with a deuteron ion (D^+) beam current of 300 μA, and the energy of the deuteron ion beam was approximately 300 keV. The thickness of solid deuterium-titanium target used in the generator was approximately 1 mg/cm^2. The yield of CPNG-600 was approximately 7.5×10^8 n/s. An Au-Si surface barrier detector was installed at 135° with respect to the D+ beam. The associated protons of the D(d, p)T reaction, representing the neutron of D(d, n)^{3}He, were recorded every 300 s to determine the neutron fluency fluctuation.

C. Sample irradiation and neutron energy determination

Potassium-bearing samples SK01 sanidine, containing 8.62% potassium, were provided by IGGCAS [24]. The selected SK01 sanidine samples are standard materials used in ^{40}Ar/^{39}Ar geochronology and widely applied in age determination. The detailed parameters of samples are shown in Table 2. The information of the main reaction ^{39}K(n, p)^{39}Ar is shown in Table 4. Three samples were packed into circular discs of 20 mm diameter. Each labeled sample was sandwiched between two nickel foils (99.99% purity, each 0.5 mm thick) of the same diameter, which served as neutron flux monitors. The assembled Ni–SK01–Ni structures were wrapped with plastic film. The wrapped samples were placed at 0°, 45°, 90° relative to the D^+ beam direction and center of the D-Ti target at a distance of approximately 4 cm. A placement diagram of the sandwiched samples is shown in Fig. 1.

The neutron mean energy emitted at angle β was determined by the cross-sectional ratio method of reactions ^{64}Zn(n, p)^{64}Cu and ^{115}In(n, n')^{115m}In [25, 26] and checked with Eq. (4) based on the Q equation proposed by Luo [27]. The calculation of mean neutron energy by the geometric model is shown in Fig. 2.

$$\overline{E} = \frac{2L}{\pi R^2}\int_{\beta-\arctan(\frac{R}{L})}^{\beta+\arctan(\frac{R}{L})} E_n(\theta, E_d)\frac{\sqrt{R^2 - L^2\tan^2(\beta-\theta)}}{\cos^2(\beta-\theta)}\mathrm{d}\theta. \tag{4}$$

The Q equation is as follows:

$$E_n(\beta, E_d) = \left\{\frac{\sqrt{2E_d}}{4}\cos(\beta) + \left[\left(\frac{1}{2} + \frac{1}{8}\cos^2(\beta)\right)E_d + \frac{3}{4}Q\right]^{\frac{1}{2}}\right\}^2. \tag{5}$$

β is the angle between the d^+ beam direction and line

Table 2. Sample information.

Sample	Number	Diameter/mm	Mass/mg
SK01	1#	20	204.9
	2#	20	204.1
	3#	20	209.5

The nickel samples were also cut into discs with a diameter of 20 mm.

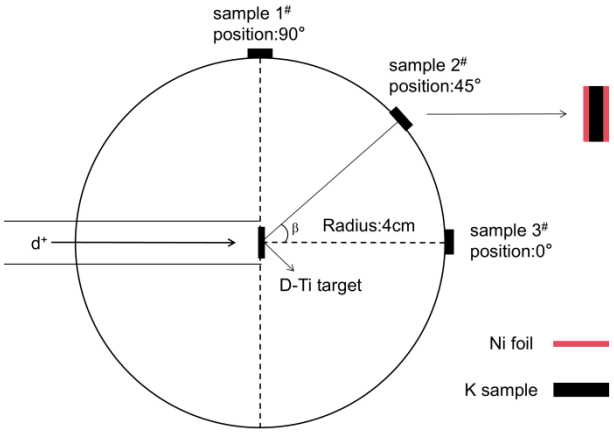

Fig. 1. (color online) Geometric model of sample and d-d generator.

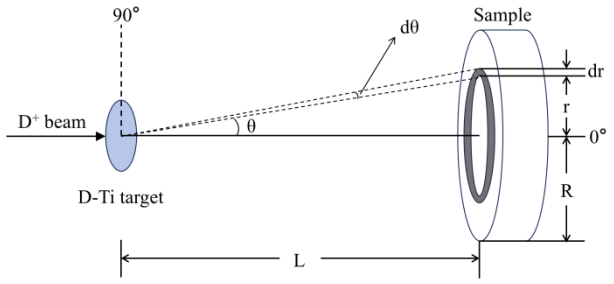

Fig. 2. (color online) Schematic diagram of mean energy calculation by the geometric model.

from the D-Ti center to sample center. The mean neutron energies of samples 1, 2, and 3 were calculated as 2.56±0.08 MeV, 2.69±0.08 MeV, and 2.96±0.12 MeV, respectively.

D. Measurement of neutron flux by ^{58}Ni activity

^{58}Ni and ^{54}Fe isotopes are found to be suitable neutron flux monitors as the cross-sections of ^{58}Ni(n, p)^{58}Co and ^{54}Fe(n, p)^{54}Mn are similar to that of ^{39}K(n, p)^{39}Ar at 2–3 MeV (the cross-sections of these reactions are shown in Fig. 3). The neutron flux detected by a similar cross-section was closer to the actual neutron flux when the sample was irradiated. The isotopic abundance of ^{54}Fe is only 5.845%, while that of ^{58}Ni is 68.077%, and the characteristic gamma-ray intensities of products ^{58}Co and ^{54}Mn are similar. Under the same mass and irradiation conditions, a large number of radioactive product nuclei can be generated from nickel foil, and more γ-ray full-energy peak signals will be detected, reducing the statistical error. If ^{54}Fe is enriched, the preparation would be difficult, and the cost would be high. Considering the simplicity and low cost of the experiment, ^{58}Ni and ^{58}Ni(n, p)^{58}Co were chosen as the isotope and reaction, respectively, to monitor neutron flux. The neutron flux was determined by the gamma spectrum of activated nickel samples, using a low-background γ-ray spectrometer

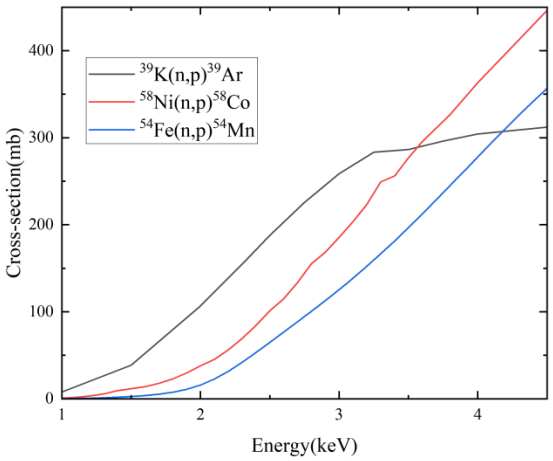

Fig. 3. (color online) Cross-sections of ^{39}K(n, p)^{39}Ar, ^{58}Ni(n, p)^{58}Co, and ^{54}Fe(n, p)^{54}Mn at neutron energy of 1–4.5 MeV.

equipped with a high-resolution HPGe detector. The decay γ-ray was emitted by ^{58}Co from the activation reaction ^{58}Ni(n, p)^{58}Co of nickel samples.

The GEM60P type HPGe detector (provided by Department of Nuclear Physics, CIAE) has a relative efficiency of 68% and a resolution of 1.82 keV at 1.33 MeV energy.^{58}Ni was chosen for the activity detection of neutron flux because the cross-section excitation function of ^{58}Ni(n, p)^{58}Co is similar to that of ^{39}K(n, p)^{39}Ar at 2–3 MeV energy, which reduces system errors. The activated nickel samples were placed 15 cm away from the detector, the dead time was less than 0.5%, and the decay γ-ray spectrum of neutron activation product ^{58}Co was detected and unfolded by energy spectrum analysis software MAESTRO from ORTEC (USA).

Neutron activation analysis time was divided into 3 parts as T_1, T_2, and T_3. T_1 is the irradiation time, T_2 is the cooling time from the end of irradiation to the start of gamma spectrum detection, and T_3 is the measurement time of gamma spectrum detection. According to the parameters of the monitor and full-energy peak γ-ray spectrum diagram from off-line γ-ray spectrometry, the equation for neutron activation analysis is as follows:

$$FC = \frac{KMN_A\eta\varphi\sigma I_\gamma\varepsilon^{\rm p}}{\lambda A}SD, \tag{6}$$

where the neutron flux is calculated by

$$\varphi = \frac{FC\lambda A}{KMN_A\eta\sigma I_\gamma\varepsilon^{\rm p}SD}. \tag{7}$$

For a reaction of $X(n, b)Y$, where M is the mass of the sample, A is the atomic weight of the parent nucleus, η is the abundance of X, σ is the cross-section of $X(n, b)Y$, φ is the mean neutron flux, I_γ is the decay γ-ray intensity of activated monitor ^{58}Co , λ is the decay constant, $N_{\rm A}$ is the

Avogadro constant, ε^p is the full-energy peak efficiency, C is the total counts in the γ-ray full-energy peak, $S=(1-e^{-\lambda T_1})$ is the growth factor, and $D=e^{-\lambda T_2}(1-e^{-\lambda T_3})$ is the counting collection factor.

F is the total correction factor of the activity, $F=F_s\times F_c\times F_g$, where Fs, Fc, and Fg are γ-ray self-absorption, γ-ray coincidence summing effects, and sample geometry factor, respectively.

K is the neutron fluency fluctuation factor [28]:

$$K=[\sum_{i}^{L}\varphi_i(1-e^{-\lambda\Delta t_i})e^{-\lambda T_i}]/\varphi S. \tag{8}$$

In this study, we divided total irradiation time into L parts, where L is the number of time intervals into which the irradiation time is divided. Δt_i is the duration of the ith time interval, T_i is the time interval from the end of the ith interval to the end of irradiation, φ_i is the neutron flux averaged over the sample during Δt_i, and φ is the neutron flux averaged over the sample during the total irradiation time T. Long time neutron irradiation of 94.5 h may cause neutron flux fluctuation; therefore, we calculated the K factor by detecting the associated proton particles, which represents the neutron flux in L parts of time, to fix results. The recorded time Δt_i was set 300 s in each of the L parts.

The differences in neutron flux measurement caused by the self-absorption effect were taken into account. The first to consider was the self-absorption effect of gamma rays. The formula of the self-absorption coefficient F_s is

$$F_s=\frac{1-e^{-\mu(E)x}}{\mu(E)x}, \tag{9}$$

where $\mu(E)$ is the energy-dependent mass attenuation coefficient ($cm^2\cdot g^{-1}$), E=810.67 keV.

x is the mass thickness, $x=\rho d$, ρ is the density of nickel, and d is the thickness of the Ni sheet.

Second, there is neutron attenuation in the SK01 sample, which is neutron self-absorption. We separately calculated the neutron flux of two sandwiched Ni sheets in each sample. According to the neutron attenuation effect, the average neutron flux of the sample is calculated by

$$\overline{\varphi}=\varphi_1\left(\frac{1-e^{-\omega s}}{\omega s}\right), \tag{10}$$

where $\overline{\varphi}$ is the average neutron flux of the sample, φ_1 is the neutron flux determined by Ni close to the D-Ti target, ω is the linear attenuation coefficient, $s=h_2$-h_1, h_1 is the distance between the center of the D-Ti target and Ni sheet close to the D-Ti target, and h_2 is the distance between the center of the D-Ti target and Ni sheet far away from the D-Ti target.

In this study, the linear attenuation coefficient was determined by

$$\varphi_2=\varphi_1\frac{h_1^2}{h_2^2}e^{-\omega s}, \tag{11}$$

where φ_2 is the neutron flux determined by Ni far away from the D-Ti target. Some of the self-absorption parameters of Sample 3$^{\#}$ are listed in Table 3.

Table 3. Self-absorption parameters of Sample 3$^{\#}$.

Parameter symbol	Value
$\mu(E)$	6.846×10^{-2} cm^2/g
x	0.445 g/cm
h_2	5.25 mm
h_1	4.25 mm
s	1 mm
ω	0.803 cm^{-1}

The gamma self-absorption factor F_s = 1.0153, which results in an increase of approximately 1.5% in the calculated neutron flux. When taking into account the neutron self-absorption effect, in comparison with the values obtained when not considering it, the neutron flux of sample 3$^{\#}$ decreases by approximately 4%, and the neutron fluxes of samples 1$^{\#}$ and 2$^{\#}$ decrease by less than 1%. Overall, the impact of self-absorption on the final measured cross-section is approximately 2.5% for sample 3$^{\#}$ and less than 1% for samples 1$^{\#}$ and 2$^{\#}$.

The detection efficiency ε^p was determined by the well-known standard source ^{152}Eu placed 15 cm from the HPGe detector, using Eq. (12):

$$\varepsilon^p=\frac{C'}{A_0 I_\gamma t\exp(-\lambda T)}, \tag{12}$$

where C' is the net count of the ^{152}Eu full energy peak in counting time t, A_0 is the source activity at time of manufacturing, T is the time from the data of manufacturing to the start time of detection, λ is the decay constant of the standard source, and I_γ is the intensity of the characteristic γ-ray.

The detection efficiency was obtained by γ-ray full-energy counts of standard source ^{152}Eu. The half-life and radioactive activity at the manufacturing time of the standard source ^{152}Eu were 13.517 a and 132192 Bq, respectively. There is a linear relationship between energy and ε under the exponential form. The fitting formula is as follows:

$$\ln(\varepsilon) = \sum_{j=1}^{n} a_j (\ln(E/E_0))^{j-1}. \quad (13)$$

where a_j is the fitting parameter, and the goodness of fit value is observed for j=3 with $\frac{\chi_j^2}{(11-3)} \approx 1$ [29]. Setting E_0 = 1 keV for simplicity, the polynomial function is given as

$$\ln(\varepsilon) = -3.3454 + 0.03015\ln(E) - 0.06037(\ln(E))^2. \quad (14)$$

The R square value is 0.997.

σ in Eq. (7) is the standard cross-section of ^{58}Ni(n, p)^{58}Co determined by the mean energy calculated by Eq. (4). The cross-sections of the activation reaction ^{58}Ni(n, p)^{58}Co were 109.38±12.18 mb, 131.76±16.12 mb, and 178.65±19.80 mb relative to the calculated neutron mean energies of 2.56±0.08 MeV, 2.69±0.08 MeV, and 2.96±0.12 MeV, respectively, from the ENDF/B-VIII.0 [15] database.

The measured ^{58}Co γ-ray spectrum is shown in Fig. 4. The constants of Ni samples are listed in Table 4. The above measured data were used in Eq. (7) to calculate the mean neutron flux.

E. ^{39}Ar content detection using noble gas mass spectrometry

Ar isotopic analyses were carried out in a noble gas laboratory at Institute of Geology and Geophysics, Chinese Academy of Sciences (IGGCAS, Fig. 5). Samples were step-heated from 970 to 1300 ℃ in 10–50 ℃ increments to release the gases. During each step, noble gases, H_2O, CO_2, and various hydrocarbons were released concurrently. Liquid-nitrogen traps removed H_2O and CO_2, and GP50 SAES getters further stripped hydrocarbons before the purified gas entered the mass spectrometer. However, residual hydrocarbons still influenced the low-abundance isotope ^{39}Ar. Argon isotopes were measured with a Noblesse multi-collector mass spectrometer. The instrument is equipped with a Nier-type ion source, a 240 mm radius magnet, one Faraday cup, and three electron multipliers. The ^{40}Ar sensitivity of the mass spectrometer is 1.2×10^{-3} A/Torr, with a mass resolution greater than 700. Isotopes were acquired in peak-jump mode. ^{40}Ar was recorded on the Faraday cup, whereas ^{39}Ar, ^{38}Ar, ^{37}Ar, and ^{36}Ar were measured on the multipliers in ion counting mode. Data reduction included blank subtraction, mass-discrimination correction, interference correction, and correction for the ^{40}Ar peak tail. A procedural blank, following the same extraction sequence as the samples, was run before each unknown. The ^{40}Ar blank contribution was <1 %, and the ^{38}Ar and ^{36}Ar blanks were <5 % of the respective signals. Air calibrations ("air shots") were used to monitor instrumental mass discrimination. The discrimination factor averaged 0.9985 ± 0.0052. Interferences on ^{39}Ar (*e.g.*, $H_2{}^{37}Cl$, C_3H_3) [30] were minimized by precise peak centering and subsequently corrected (Fig. 6). Because ^{40}Ar is 4–5 orders of magnitude more abundant than ^{39}Ar, the effect of ^{40}Ar tailing on the adjacent ^{39}Ar peak was evaluated. Tests on atmospheric standards devoid of ^{39}Ar showed that ^{40}Ar tailing contributed <0.3 ppm to the apparent ^{39}Ar signal. Corrected ^{39}Ar abundances are reported in Table 5.

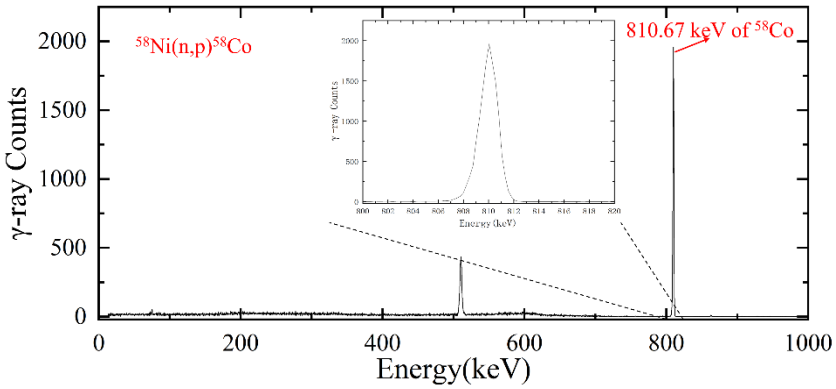

Fig. 4. (color online) Typical γ-ray spectrum of ^{58}Co measured by off-line γ-ray spectrometer equipped with HPGe detector.

Table 4. Main reaction data of irradiated samples.

Reaction	Abundance of target isotope η (%)[a]	Half-life of product $T_{1/2}$	γ-ray energy E_γ (keV)[b]	γ-ray intensity I_γ (%)[c]
^{58}Ni(n, p)^{58}Co	68.007	70.860d	810.759	99.45
^{39}K(n, p)^{39}Ar	93.258	268y	-	-

a. The abundance of target isotope represents ^{58}Ni and ^{39}K isoptopes of natual elements in samples. b. The half-lives of products represent the half-lives of ^{58}Co and ^{39}Ar in irradiated samples. c. The γ-ray energy and intensity are those of the decay γ-rays of the ^{58}Co product.

Fig. 5. (color online) Photo of Noble gas laboratory in IGGCAS.

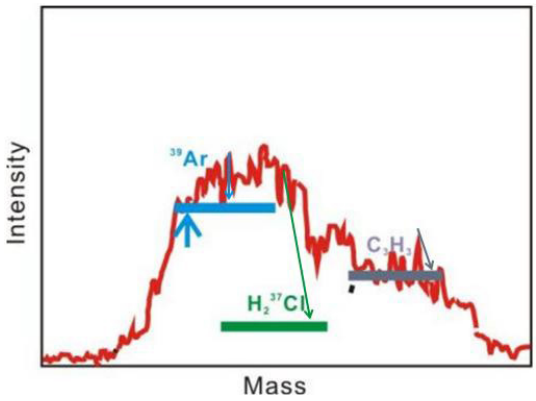

Fig. 6. (color online) Schematic diagram of the peak position of mass number 39, where the blue, green, and purple lines are the peak widths of ^{39}Ar, $H_2{}^{37}Cl$, and C_3H_3, respectively, and the blue arrows are the measured positions of ^{39}Ar, independent of interference.

III. THEORETICAL CALCULATION OF COMPUTER CODE TALYS

TALYS is a computer program that can analyze the nuclear reaction cross-sections of protons [31], neutrons, photons, deuterons, tritons, and ^{3}He and α particles in the eV-200 MeV energy range and target nuclei masses of 12 or heavier. The cross-sections can be obtained considering an optical model for direct reactions, pre-equilibrium reactions, and compound reactions in TALYS-1.97. The optical model potential parameters for neutrons were obtained by local and global parameterizations of Koning and Delaroche [32]. The direct reaction contribution was considered and calculated with Distorted Wave Born Approximation (DWBA) using ECIS-06 code. The two-component exciton model developed by Kalbach [33] was used for calculating pre-equilibrium reaction contribution. The compound reaction contribution was processed using the Hauser-Feshbach statistic model with width fluctuation of the Moldauer expression model [34, 35]. The default values were used for parameters concerning nuclear masses, discrete levels, pre-equilibrium, and photon strength functions in the TALYS calculation, and the level densities and optical model were adjusted (ldmodel 2, rvadjust n 1.16, avadjust n 1.04, rwdadjust n 0.98, awdadjust n 0.98). The theoretical data achieved a high consistency with the evaluated data at low and high energies and achieved a high consistency with the experimental data at medium energy (4–9 MeV). Meanwhile, all other outgoing channels were considered to include (n, α) induced reactions and inelastic scattering. The cross-sections of ^{39}K(n, p)^{39}Ar were simulated by TALYS-1.97 with the energy reaching up to 20 MeV.

Table 5. Measured ^{39}Ar content of samples.

Sample No.	^{39}Ar content/mol
1#	$(6.96\pm0.44)\times10^{-17}$
2#	$(1.11\pm0.06)\times10^{-16}$
3#	$(4.58\pm0.29)\times10^{-16}$

IV. RESULTS AND DISCUSSION

A. Results

The cross-sections of ^{39}K(n, p)^{39}Ar were determined by the measured content of ^{39}Ar and the characteristic γ-ray full-peak counts of the activated monitor γ-ray spectrum. The mean neutron energy, total neutron fluence Φ_{tot}, ^{39}Ar content, and ^{39}K(n, p) reaction cross-sections values measured for each sample are summarized in Table 6 according to the sample number. The cross-sections of samples are 103.84±16.33 mb, 109.76±15.88 mb, and 150.27±24.19 mb at mean neutron energies of 2.56±0.08 MeV, 2.69±0.08 MeV, and 2.96±0.12 MeV, respectively. The measured cross-sections in this study are plotted in Fig. 7 and Fig. 8 along with the already existing experimental data reported in the EXFOR database. Moreover, the present results are compared with evaluated nuclear data from ENDF/B-VIII.0, JEFF-3.3, TENDL-2021, BROND-3.1, and JENDL-5 databases and the TALYS-1.97 code.

B. Uncertainty

The uncertainties of neutron flux are caused by detection efficiency of the HPGe detector and the mean neutron energy.

The detection efficiency ε^p is calculated by Eq. (12); according to the polynomial fitting results, the uncertainty of detection efficiency at 810.67 keV is approximately 3%. The monitor reaction cross-section uncertainty is approximately 5.2%, because of neutron mean energy calculated by the angle β and diameter of sample. The uncertainty of neutron fluence is calculated to be approximately 2.5%. The uncertainty of counting statistics is 0.8%.

Table 6. Experimental data of ^{39}K(n, p)^{39}Ar cross-sections.

Sample No.	Values and results				
	M /mg	E_n /MeV	Φ_{tot} /(n·cm^{-2})	^{39}Ar/mol	σ_K/mb
1#	204.9	2.56±0.08	1.48×10^{12}	6.96×10^{-17}	103.84±16.33
2#	204.1	2.69±0.08	2.24×10^{12}	1.11×10^{-16}	109.76±15.88
3#	209.5	2.96±0.12	6.58×10^{12}	4.58×10^{-16}	150.27±24.19

σ_K means the cross-section of ^{39}K(n, p)^{39}Ar.

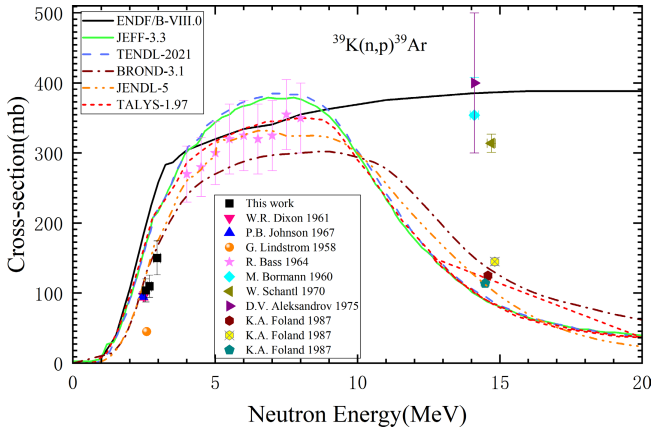

Fig. 7. (color online) Data comparison of ENDF/B-VIII.0, JEFF-3.3, TENDL-2021, BROND-3.1, JENDL-5, TALYS-1.9 model code, other experiments, and this work.

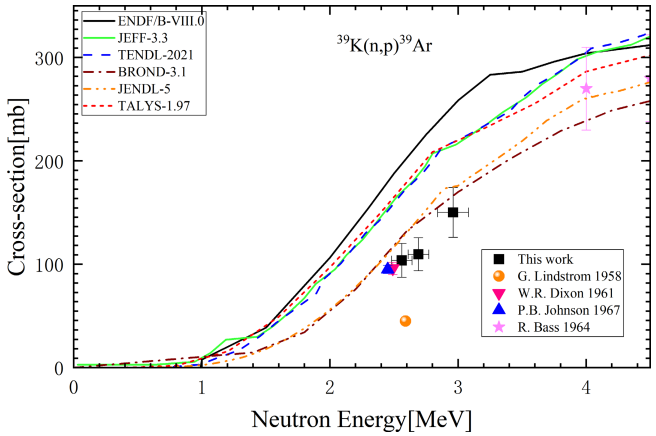

Fig. 8. (color online) Cross-sections of ^{39}K(n, p)^{39}Ar in the 0–4.5 MeV mean neutron energy region.

The total correction factors of the activity F are the self-absorption of γ-ray (~1%), the coincidence summing effect of cascade γ-rays (~1%), and the sample geometry (~1%). The weight of samples is less than 0.1%. The neutron fluency fluctuation factor K is approximately 0.1%. The uncertainty of the Ar isotope measurement is approximately 6% due to the low abundance of mass 39 elements and the uncertainty of the volume of the measuring system. The uncertainties are listed in Table 7 for reference. The total uncertainty was calculated by the quadratic method.

Table 7. Uncertainties of ^{39}K(n, p)^{39}Ar cross-section.

Source of Unertainty	Symbol	Estimated Values (%)	Remarks
Counting statistics	C	0.8	Calculated by $1/\sqrt{C}$
Weight of samples	M	<0.1	
Detection efficiency	ε^p	3	
Self-absorption	F_s	1	
Coincidence summing effect	F_c	1	
Sample geometry	F_g	1	
Neutron fluency fluctuation	K	0.1	
Times	T	1.6	Including irradiation(T_1), cooling(T_2), measuring(T_3) times
Cross-section of ^{58}Ni(n, p)^{58}Co	σ_{Ni}	5.2	
Neutron fluence	Φ_{tot}	2.5	
^{39}Ar isotope measurements	^{39}Ar	6	

The detection of argon content contributed most of the uncertainty, mainly because the ^{39}Ar produced by neutron irradiation was insufficient and only slightly higher than the background mass of 39. ^{39}Ar yield was determined by the irradiation neutron flux and time. The irradiation time took into account the half-life of the activation monitor and yield of argon. The neutron flux was bound by the neutron source intensity of CPNG-600, which was 7.5×10^8 n/s in this study. The neutron flux generated at the samples was relatively low and coupled with the time limitation, making the ^{39}Ar products insufficient.

C. Discussion

Compared with the available cross-sections in literature and the evaluation databases shown in Fig. 7, the measured data complied better with the law that cross-sections increase rapidly in the energy range of 2–3 MeV. To more clearly compare the measured data with those of other research and evaluated data, we enlarged the image in the energy range of 1–4.5 MeV, as shown in Fig. 8. In addition, the excitation function calculated by TALYS-

1.97 is shown in Fig. 7 and Fig. 8, which closely agrees with the evaluated data curves of JEFF-3.3 and TENDL-2021. The measured data in this study are close to the data measured by Dixon in 1961, clarifying the data deviation between Lindström and others. It is highly likely that, as Johnson [6] inferred, in the paper of Lindström, the (n, α) and (n, p) double peaks are actually a single peak of (n, p). After treating it as a single peak, the cross-section of 81 mb is still much lower than the evaluation value. The main reason can be inferred as follows: the deuterium signal and other non-^{3}He signals were confused with the ^{3}He signal, resulting in an overestimation of the ^{3}He reading and ultimately the underestimation of cross-sections. The measured data in this study are close to the evaluated data of the JENDL-5 and BROND-3.1 databases. The JENDL-5 database focuses more on the fitting of experimental data and the evaluation of covariance data [19]. The measured cross-sections are consistent with the physical laws and close to the evaluation excitation function and previously published experimental data, which shows that our proposed detection method of combined NAA and NGMS techniques to measure the absolute matter content and neutron flux for determination of cross-sections is feasible and reliable.

The black filled squares are the data determined in this study. The error regarding energy is relatively small, and the error bars are covered by the data points. In the following illustration, they are enlarged for easier reference.

In the enlarged figure, only the data points and legends within the energy range of 0–4.5 MeV are retained, and the retained legends are consistent with Fig. 7.

V. CONCLUSION

In the present study, the cross-sections of the ^{39}K(n, p)^{39}Ar reaction were determined by the combined NAA and NGMS detection method. The cross-section data were obtained by the activated sample and monitor as 103.84±16.33, 109.76±15.88, and 150.27±24.19 mb at mean neutron energies of 2.56±0.08, 2.69±0.08, and 2.96±0.12 MeV, respectively. Moreover, the excitation function of cross-sections was calculated theoretically by TALYS-1.97 codes. The measured cross-sections of ^{39}K(n, p)^{39}Ar were compared with the cross-sections obtained via the evaluation functions of the ENDF/B-VIII.0, JEFF-3.3, TENDL-2021, BROND-3.1, and JENDL-5 databases, previously available literature data, and the theoretical cross-section calculated by the evaluation function of TALYS-1.97.

Compared with the data reported in the EXFOR database, evaluated data from five databases, and theoretical calculation from TALYS-1.97, the measured cross-sections of ^{39}K(n, p)^{39}Ar in this study were proved to be reliable enough to fill the data gaps of databases. The absolute measurement of ^{39}K and ^{39}Ar content and γ-ray full peak counts with the high sensitivity and resolution instruments in the NAA and NGMS combined detection method avoid the peak overlap problem, and the precision of the cross-sections of the ^{39}K(n, p)^{39}Ar reaction is evidently improved by high resolution laboratory apparatus.

Although there is still a problem of insufficient argon production, the problem will be gradually solved as the neutron generator yield increases and resolution of the mass spectrometer improves. It is foreseeable that the method combining NAA and NGMS will be more accurate in measuring neutron reaction cross-sections in the future. Furthermore, the combined method of NAA and NGMS can be applied to the process of ^{40}Ar/^{39}Ar dating to replace nuclear reactor irradiation and improve the problems of Ar nuclear recoil and excessive interference reactions.

ACKNOWLEDGMENTS

The authors are grateful to the staff of the CPNG-600 neutron generator at China Institute of Atomic Energy for their assistance with daily maintenance and operation. The authors also thank the staff of the Noblesse noble gas mass spectrometer at Institute of Geodesy and Geophysics, Chinese Academy of Sciences, for their assistance with maintenance.

References

[1] C. Wen, Z. Han, and X. B. Luo, Chin. Phys. C **47**, 024002 (2023)
[2] D. B. Nichols, and M. T. McEllistrem, Phys. Rev. **166**, 1074 (1968)
[3] G. Lindström, and H. Neuert, Z. Naturforsch. A **13**, 826 (1958)
[4] W. R. Dixon, and J. H. Aitken, Nucl. Phys. **24**, 456 (1961)
[5] R. Bass, U. Fanger, and F. M. Saleh, Nucl. Phys. **56**, 569 (1964)
[6] P. B. Johnson, N. G. Chapman, and J. E. Callaghan, Nucl. Phys. A **94**, 617 (1967)
[7] P. L. Okhuysen, E. W. Bennett, J. B. Ashe *et al*., Rev. Sci. Instrum. **29**, 982 (1958)
[8] P. Shapiro, and R. W. Higgs, Phys. Rev. **108**, 760 (1957)
[9] W. Franzen, P. Huber, and L. Schellenberg, Z. Naturforsch. A **10**, 820 (1955)
[10] S. Kelley, Rev. Mineral. and Geochem **47**, 785 (2002)
[11] P. R. Renne, K. B. Knight, S. Nomade *et al*., Appl. Radiat. Isot. , **62**, 25 (2005)
[12] I. Osborne, S. Sherlock, M. Anand *et al*, Precambrian Res. **189**, 91 (2011)
[13] D. P. West Jr, and D. R. Lux, Earth Planet. Sci. Lett. **120**,

221 (1993)
[14] S. Kelley, Chem. Geol. **188**, 1 (2002)
[15] D. A. Brown, M. B. Chadwick, R. Capote *et al*., Nucl. Data Sheets **148**, 1 (2018)
[16] A. J. M. Plompen, O. Cabellos, C. De Saint Jean *et al*., Eur. Phys. J. A **56**, 181 (2020)
[17] A. J. Koning, D. Rochman, J. Sublet, *et al*., Nucl. Data Sheets **155**, 1 (2019)
[18] A. I. Blokhin, E. V. Gai, A. V. Ignatyuk *et al*., Yad. Reak. Konst. **2**, 62 (2016)
[19] O. Iwamoto, N. Iwamoto, S. Kunieda *et al*., Nucl. Sci. Tech. **60**, 1 (2023)
[20] C. L. Lan, X. L. Yang, X. J. Li *et al*., Nucl. Instrum. Methods Phys. Res. Sect. B **525**, 18 (2022)
[21] C. L. Lan, Y. X. Niu, Y. T. Wei *et al*., Chin. Phys. C **47**, 094001 (2023)
[22] D. F. Mark, D. Barfod, F. M. Stuart *et al*., Geochem. Geophys. Geosyst. **10**, Q0AA02 (2009)
[23] D. He, F. M. Stuart, D. N. Barfod *et al*., Acta Geochim. **37**, 734 (2018)
[24] L. Jie, C. Wen, X. Liu *et al*., Rock Miner. Anal. **32**, 213 (2013)
[25] T. Shimizu, H. Sakane, S. Furuichi *et al*., Nucl. Instrum. Methods Phys. Res. Sect. A **527**(3), 543 (2004)
[26] Y. J. Ge, C. L. Lan, H. Y. Lv *et al*., Appl. Radait. Isotopes **200**, 110907 (2023)
[27] J. H. Luo, Nucl. Instrum. Meth. B **359**, 5 (2015)
[28] C. L. Lan, X. S. Xu, K. H. Fang *et al*., Ann. Nucl. Energy **35**, 2105 (2008)
[29] S. Y. Sheela, H. Naik, K. M. Prasad *et al*. , Internal Report no. Mu/Stastics/DAE-BRNS/2017, 2017
[30] M. A. Coble, M. Grove, and A. T. Calvert, Chem. Geol. **290**, 75 (2011)
[31] A. J. Koning, S. Hilaire, and S. Goriely, Eur. Phys. J. A **59**, 131 (2023)
[32] A. J. Koning and J. P. Delaroche, Nucl. Phys. A **713**, 231 (2003)
[33] C. Kalbach, Phys. Rev. C **33**, 818 (1986)
[34] H. M. Hofmann, T. Mertelmeier, M. Herman, *et al*., Zeit. Phys. A **297**, 153 (1980)
[35] P. A. Moldauer, Nucl. Phys. A **344**, 185 (1980)